

# TiH<sub>2</sub> Nanodots Exfoliated via Facile Sonication as Bifunctional Electrocatalysts for Li–S Batteries

Tianran Yan, Yu Wu, Fei Gong, Chen Cheng, Hao Yang, Jing Mao, Kehua Dai, Liang Cheng,\* Tao Cheng,\* and Liang Zhang\*



Cite This: *ACS Appl. Mater. Interfaces* 2022, 14, 6937–6944



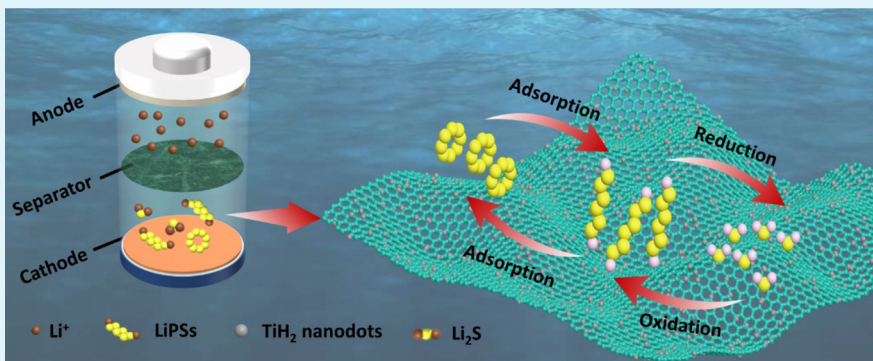
Read Online

ACCESS |

Metrics & More

Article Recommendations

Supporting Information



**ABSTRACT:** Mediating the redox kinetics of polysulfides is a promising strategy to mitigate the shuttling and sluggish conversion of polysulfides for practical application of lithium–sulfur (Li–S) batteries. Herein, novel TiH<sub>2</sub> nanodots (THNDs) fabricated by sonication-assisted liquid-phase exfoliation are used as bifunctional electrocatalysts for Li–S batteries. Both experimental and theoretical results reveal that THNDs can not only provide a strong chemical affinity to polysulfides but also bidirectionally promote the precipitation/decomposition of Li<sub>2</sub>S from/to polysulfides during the discharge/charge process, thus effectively suppressing the shuttle effect and improving the redox kinetics of polysulfides. Owing to these advantages accompanied by the abundant catalytically active sites of THNDs, the assembled Li–S batteries deliver a low capacity fading rate of 0.055% per cycle over 1000 cycles at 1C and a high areal capacity of 5.38 mAh cm<sup>-2</sup> after 50 cycles with a high sulfur loading of 8.5 mg cm<sup>-2</sup>. This work demonstrates the great potential of utilizing functional metal hydrides as effective electrocatalysts for Li–S batteries, which will incite more investigation into the specific selection of metal compounds to boost the redox kinetics of polysulfides.

**KEYWORDS:** *Li–S batteries, TiH<sub>2</sub> nanodots, shuttle effect, bifunctional electrocatalyst, redox kinetics*

## INTRODUCTION

As one of the most promising next-generation energy-storage systems, lithium–sulfur (Li–S) batteries have attracted extensive attention.<sup>1–3</sup> Despite their intriguing merits of low cost, environmental friendliness, and high theoretical energy density,<sup>4</sup> the development of Li–S batteries is largely hindered by the shuttling and sluggish conversion of lithium polysulfides (LiPSs), which results in rapid capacity decay and a poor lifetime.<sup>5,6</sup> To address the obstacles mentioned above, considerable efforts have been devoted to the design of cathode materials by encapsulating the active sulfur materials with conductive polar host materials to suppress the shuttling of LiPSs.<sup>7–10</sup> However, this strategy inevitably introduces a large number of inactive host materials in the cathodes, which do not contribute to the capacity at all and therefore significantly reduce the energy density.<sup>11</sup> Typically, up to 30–60 wt % of host materials are required to effectively suppress LiPSs shuttling in composite cathodes, implying an

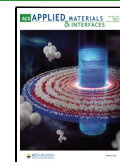
energy loss of ~20 to 50% compared to pure S/carbon black cathodes with 70% S loading.<sup>12</sup> Worse still, due to the tedious manufacturing process as well as the unsatisfactory cycling performance at a high sulfur loading condition, the complicated cathode design strategies are difficult to meet the requirements of practical applications of Li–S batteries.<sup>13</sup>

In contrast, neoteric functional separators using facile preparation methods and relatively few inactive materials have gained remarkable attention to improve the electrochemical performance of Li–S batteries.<sup>14,15</sup> In this regard, various carbonaceous materials, such as graphene, carbon

Received: December 15, 2021

Accepted: January 18, 2022

Published: January 26, 2022



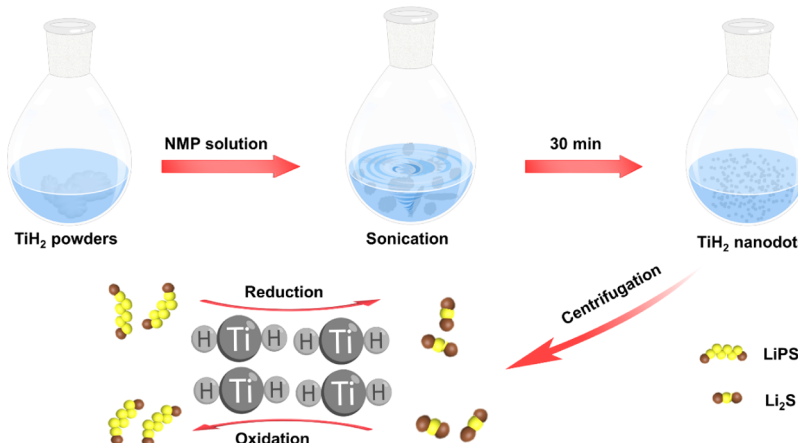


**Figure 1.** Schematic illustration of the fabrication process of THNDs and the application for Li–S batteries.

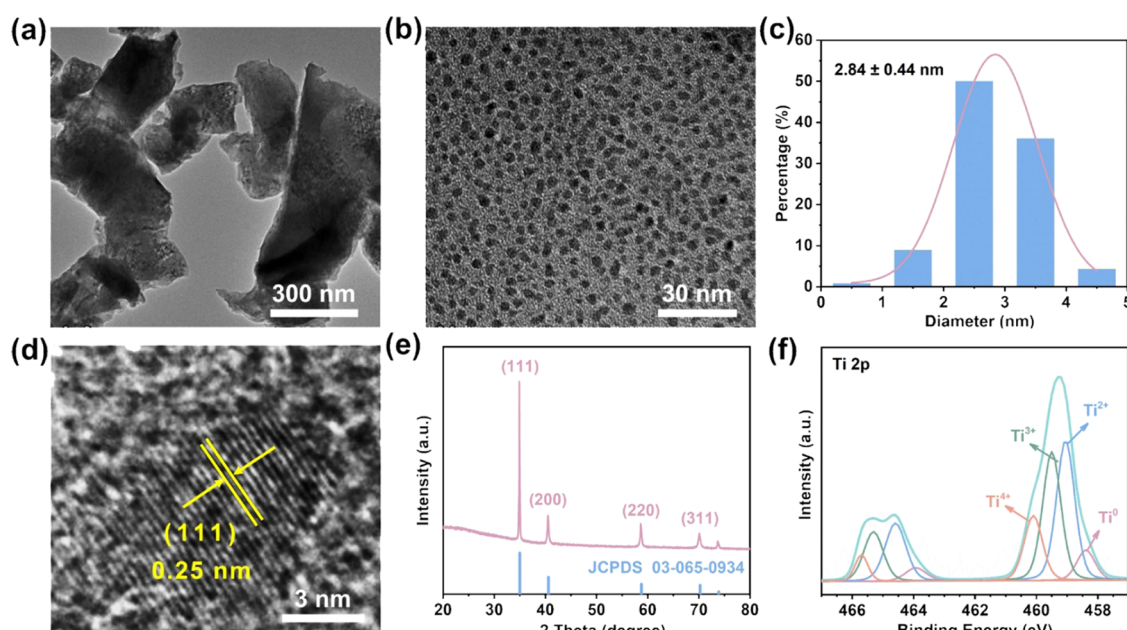


**Figure 2.** (a) TEM image of commercial  $\text{TiH}_2$  powder, (b) TEM image of THNDs, (c) particle size distribution of THNDs determined by the TEM image, (d) high-resolution TEM image of THNDs, (e) XRD pattern of THNDs, and (f) Ti 2p XPS spectrum of THNDs.

nanotubes, and carbon nanofibers, have been frequently used as coating materials to functionalize the separators due to their good electrical conductivity and light mass. However, the weak interaction between nonpolar carbonaceous materials and polar LiPSs reduces their ability to suppress the shuttle effect, especially under high sulfur loading and high current rate conditions.<sup>16</sup> More recently, it has been proposed that the introduction of metal-based electrocatalysts (metal alloys,<sup>13,17</sup> metal carbides,<sup>18</sup> nitrides,<sup>19</sup> oxides,<sup>20</sup> sulfides,<sup>21</sup> single-atom metal catalysts,<sup>22</sup> and so on<sup>23–25</sup>) can accelerate the redox kinetics of LiPSs, thereby effectively reducing their dissolution and diffusion in the electrolyte.

Materials based on metal hydrides can be utilized as media not only for hydrogen energy storage but also electrochemical energy storage, as witnessed by rapidly evolving discoveries.<sup>26–30</sup> Typically, hydrogen atoms only occupy the interstitial sites of the corresponding metal framework, while the arrangement of metal atoms remains unchanged with a slight distance increase between adjacent metal atoms. Therefore, the formed metal hydrides are less dense than the

original metals with most of the properties (such as good electrical conductivity and catalytic properties) retained.<sup>31</sup> Considering these merits of metal hydrides, we believe that they are promising electrocatalysts to functionalize the separators of Li–S batteries. However, most of the reported metal hydrides are mainly in the bulk form and it is difficult to obtain nanostructured metal hydrides, which makes it difficult to fully exploit the corresponding surface chemical reactivity and catalytic activity.<sup>32,33</sup>

Herein, we report a facile liquid-phase exfoliation strategy for scalable production of  $\text{TiH}_2$  nanodots (THNDs) as efficient LiPSs immobilizers and bifunctional electrocatalysts for functional separators of Li–S batteries. Based on the experimental and theoretical investigations, we found that THNDs can effectively immobilize the LiPSs through strong anchoring capability. In addition, THNDs could also simultaneously promote the deposition of  $\text{Li}_2\text{S}$  from LiPSs during discharge and decomposition of  $\text{Li}_2\text{S}$  during subsequent charge due to the presence of numerous catalytically active sites of the nanodots. As a consequence, the assembled Li–S

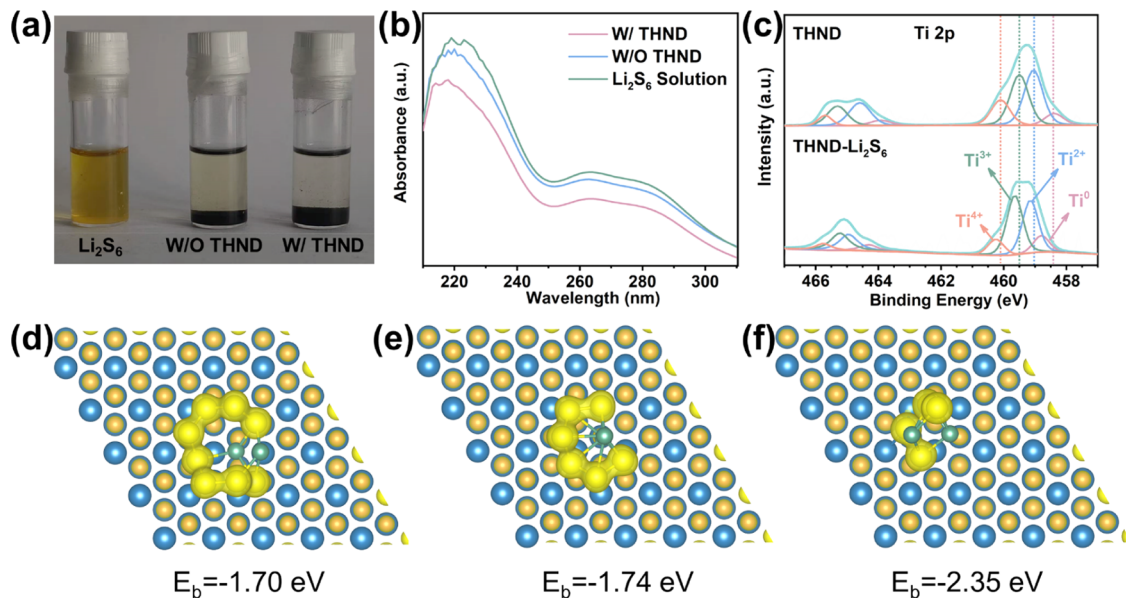


**Figure 3.** (a) Digital photograph of  $\text{Li}_2\text{S}_6$  solutions before and after interacting with THNDs; (b) UV-vis spectra of the  $\text{Li}_2\text{S}_6$  solution mixed with different samples; (c) Ti 2p XPS spectra of THNDs before and after interacting with  $\text{Li}_2\text{S}_6$ ; and DFT-optimized geometric configurations and energies of  $\text{TiH}_2$  (111) binding with (d)  $\text{Li}_2\text{S}_8$ , (e)  $\text{Li}_2\text{S}_6$ , and (f)  $\text{Li}_2\text{S}_4$ .

batteries with THNDs exhibit a high areal capacity of 5.38 mAh cm<sup>-2</sup> with a high sulfur loading of 8.5 mg cm<sup>-2</sup>, a high rate capability of 818.2 mAh g<sup>-1</sup> at 4C, and a low capacity decay of 0.055% per cycle over 1000 cycles. To the best of our knowledge, this is the first report on utilizing nanosized metal hydrides as electrocatalysts to improve the sulfur redox kinetics, which pioneers a new avenue for designing high-performance Li–S batteries.

## RESULTS AND DISCUSSION

THNDs were prepared using a simple one-step liquid-phase exfoliation method, as shown in Figure 1. First, the commercially available micron-sized  $\text{TiH}_2$  powder was added into an *N*-methyl pyrrolidone (NMP) exfoliation solution. Then, the mixture was sonicated for 30 min to obtain ultrasmall THNDs. It is worth mentioning that the similar surface energy of  $\text{TiH}_2$  and NMP plays a crucial role in the successful exfoliation of THNDs.<sup>34,35</sup>

The morphology of the as-prepared THNDs was characterized by transmission electron microscopy (TEM). Compared to the commercial  $\text{TiH}_2$  powder (Figures 2a and S2), the size of THNDs is considerably smaller and more homogeneous (Figure 2b) with an average diameter of  $2.84 \pm 0.44$  nm (Figure 2c). In addition, THNDs showed high dispersion as well as stability in NMP solutions. (Figure S2). Such an ultrafine structure is favorable for the exposure of numerous catalytic active sites, leading to the improved utilization of the electrocatalysts. The lattice spacing determined by high-resolution TEM is  $\sim 2.5$  Å (Figure 2d), which corresponds to the (111) planes of  $\text{TiH}_2$ . In addition, X-ray diffraction (XRD) patterns of THNDs (Figure 2e) can be well indexed to those of the bulk  $\text{TiH}_2$  (JCPDF 03-065-0934). This observation indicates that the formation of THNDs is only a simple physical exfoliation process without the involvement of a complex chemical reaction, which could be scaled up for the preparation of the large-amount and high-quality THNDs. X-ray photoelectron spectroscopy (XPS) results further reveal the unique valence state of THNDs with four components

including  $\text{Ti}^0$ ,  $\text{Ti}^{2+}$ ,  $\text{Ti}^{3+}$ , and  $\text{Ti}^{4+}$  (Figure 2f). The complex Ti species existing here may be due to slight oxidation of the catalyst surface,<sup>36</sup> which may provide multilevel chemisorption ability toward soluble LiPSs.

To further verify the strong trapping ability of THNDs for LiPSs, a visualized adsorption test and ultraviolet-visible (UV-vis) measurement were conducted. As shown in Figure 3a, the  $\text{Li}_2\text{S}_6$  solution containing THNDs becomes almost transparent after standing for 4 h, while the color of the  $\text{Li}_2\text{S}_6$  solution without THNDs remains yellowish, directly revealing the strong adsorption capacity of THNDs for LiPSs. Moreover, the reduced intensity of the characteristic absorption peaks of  $\text{S}_6^{2-}$  ( $\sim 260$  and  $\sim 280$  nm) also manifests the strong chemical affinity of THNDs toward LiPSs.<sup>37</sup> The intrinsic interactions between THNDs and LiPSs were also investigated by XPS. In the Ti 2p XPS spectra (Figure 3c), the binding energies of four characteristic peaks ( $\text{Ti}^0$ ,  $\text{Ti}^{2+}$ ,  $\text{Ti}^{3+}$ , and  $\text{Ti}^{4+}$ ) all shift to higher energies after  $\text{Li}_2\text{S}_6$  adsorption, confirming the strong chemical interactions between them.<sup>38,39</sup> Note that different Ti species exhibit different energy shifts after interacting with LiPSs, confirming the multilevel adsorption of THNDs toward LiPSs.

To further evaluate the interactions between THNDs and LiPSs at the atomic scale, first-principles density functional theory (DFT) calculations were conducted. The optimized conformations of the LiPS intermediates are shown in Figure S3, which are well consistent with previous results.<sup>40</sup> The optimized geometric configurations for long-chain LiPSs, namely,  $\text{Li}_2\text{S}_8$ ,  $\text{Li}_2\text{S}_6$ , and  $\text{Li}_2\text{S}_4$ , on the  $\text{TiH}_2$  (111) surface are shown in Figures 3d–f and S4.<sup>41</sup> The corresponding binding energy ( $E_b$ ) values between the  $\text{TiH}_2$  (111) surface and  $\text{Li}_2\text{S}_8$ ,  $\text{Li}_2\text{S}_6$ , and  $\text{Li}_2\text{S}_4$  are calculated to be  $-1.70$ ,  $-1.74$ , and  $-2.53$  eV, respectively, which are much higher than those of graphene surfaces (Table S1). This implies the enhanced chemical interaction between THNDs and LiPSs, which is in good agreement with the experimental results.

It has been well established that the sulfur redox reactions mainly include the liquid–liquid, liquid–solid, and solid–solid conversions, which are equally important for realizing the rapid

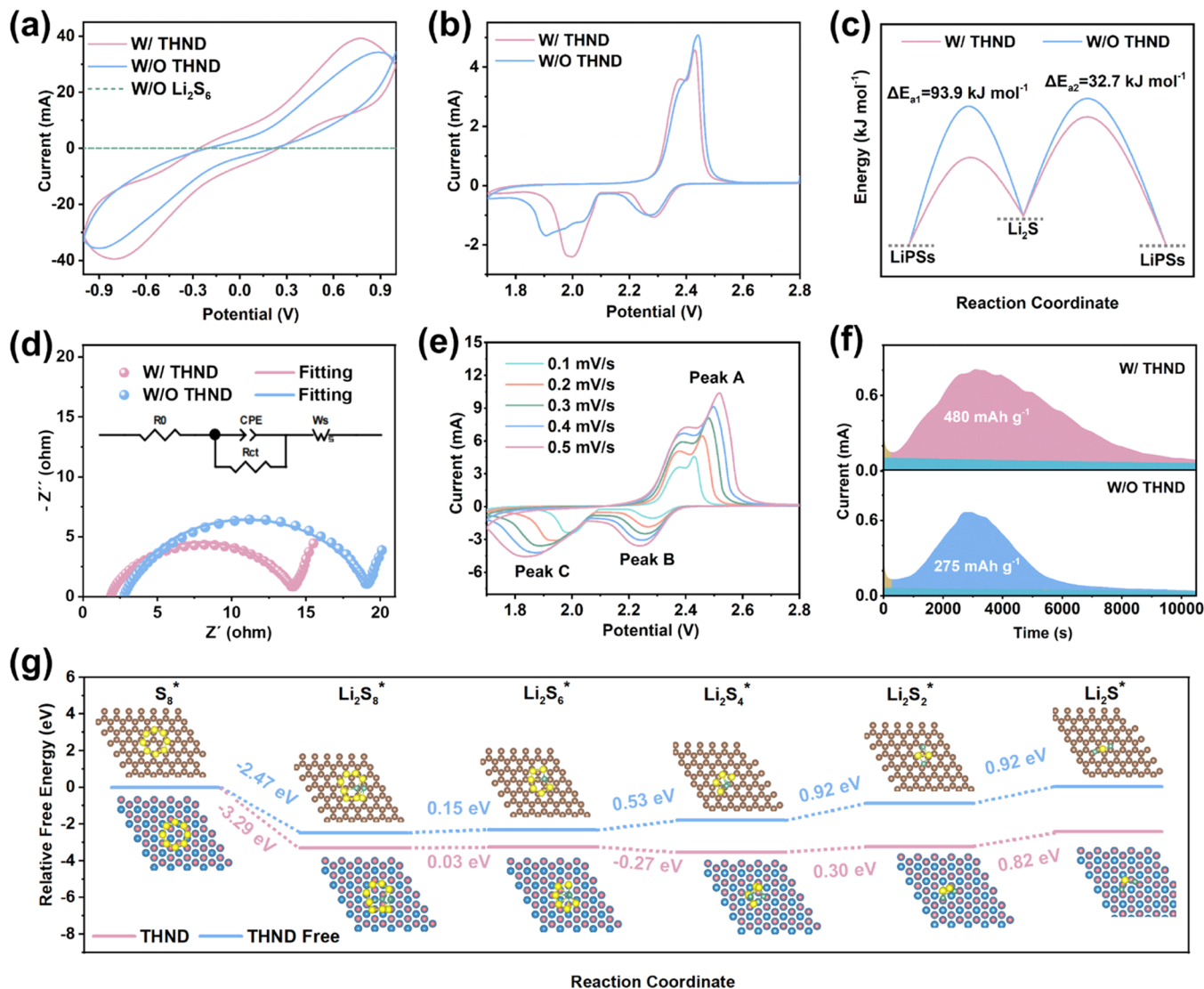


**Figure 4.** (a) CV curves of symmetrical cells with different separators, (b) CV curves of Li–S batteries with different separators, (c) calculated activation energy difference of the formation and decomposition of Li<sub>2</sub>S for Li–S batteries with different separators, (d) EIS spectra of Li–S batteries with different separators, (e) CV curves of Li–S batteries with the THNDs-modified separator at different scan rates, (f) potentiostatic discharge profiles with a Li<sub>2</sub>S<sub>8</sub> solution at 2.05 V, and (g) calculated energy profiles for the reduction of sulfur and LiPSs on graphene and THNDs. The inset images show the optimized adsorption conformations of intermediate species on graphene and THNDs.

redox kinetics of Li–S batteries.<sup>42</sup> To investigate the catalytic effect of THNDs on sulfur redox kinetics, the as-prepared THNDs were introduced to functionalize the commercial PP separators using a simple physical coating method. The thickness of the coating layer is ~10 μm with a uniform distribution (Figure S5). The THNDs-modified separators also demonstrate strong mechanical stability against repeated wrinkling and bending (Figure S6), which ensures robust long-term cycling stability. The cyclic voltammetry (CV) measurement of symmetrical cells was first performed to investigate the catalytic effect of THNDs on the liquid–liquid conversion process of sulfur species (Figure 4a). It is apparent that the THNDs-based cell displays a higher current density and smaller voltage polarization than those of the cell without THNDs, indicating that the redox conversion between liquid LiPSs is effectively accelerated by THNDs.<sup>43</sup> This is beneficial for the efficient utilization of soluble LiPSs during both charge and discharge processes.

In addition to the liquid–liquid conversion process, the liquid–solid and solid–liquid transformations were also investigated by CV measurements of Li–S batteries with and without THNDs at a scan rate of 0.1 mV s<sup>-1</sup> (Figure 4b). Both CV profiles demonstrate two cathodic peaks (~2.3 and 2.0 V) and one anodic peak (~2.4 V), which are related to the two-step reduction of sulfur to Li<sub>2</sub>S and the reverse oxidation of Li<sub>2</sub>S to sulfur, respectively. Notably, the cathodic peak at ~2.0 V for the THNDs-based battery shows a distinct positive shift compared to that without THNDs, suggesting an improved conversion from liquid LiPSs to solid Li<sub>2</sub>S on the THNDs surface. In addition, the negative shift of the anode peak implies that THNDs also promotes the decomposition of Li<sub>2</sub>S. The facilitated bidirectional liquid and solid interconversion by THNDs is further consolidated by the Tafel plots, which show distinctly smaller values for the reduction process from Li<sub>2</sub>S<sub>x</sub> to Li<sub>2</sub>S (92.96 vs 122.03 mV dec<sup>-1</sup>, Figure S7) and the oxidation process from Li<sub>2</sub>S to Li<sub>2</sub>S<sub>x</sub> (46.18 vs 68.69 mV dec<sup>-1</sup>, Figure S8).<sup>44</sup> The bidirectional catalysis of THNDs is also

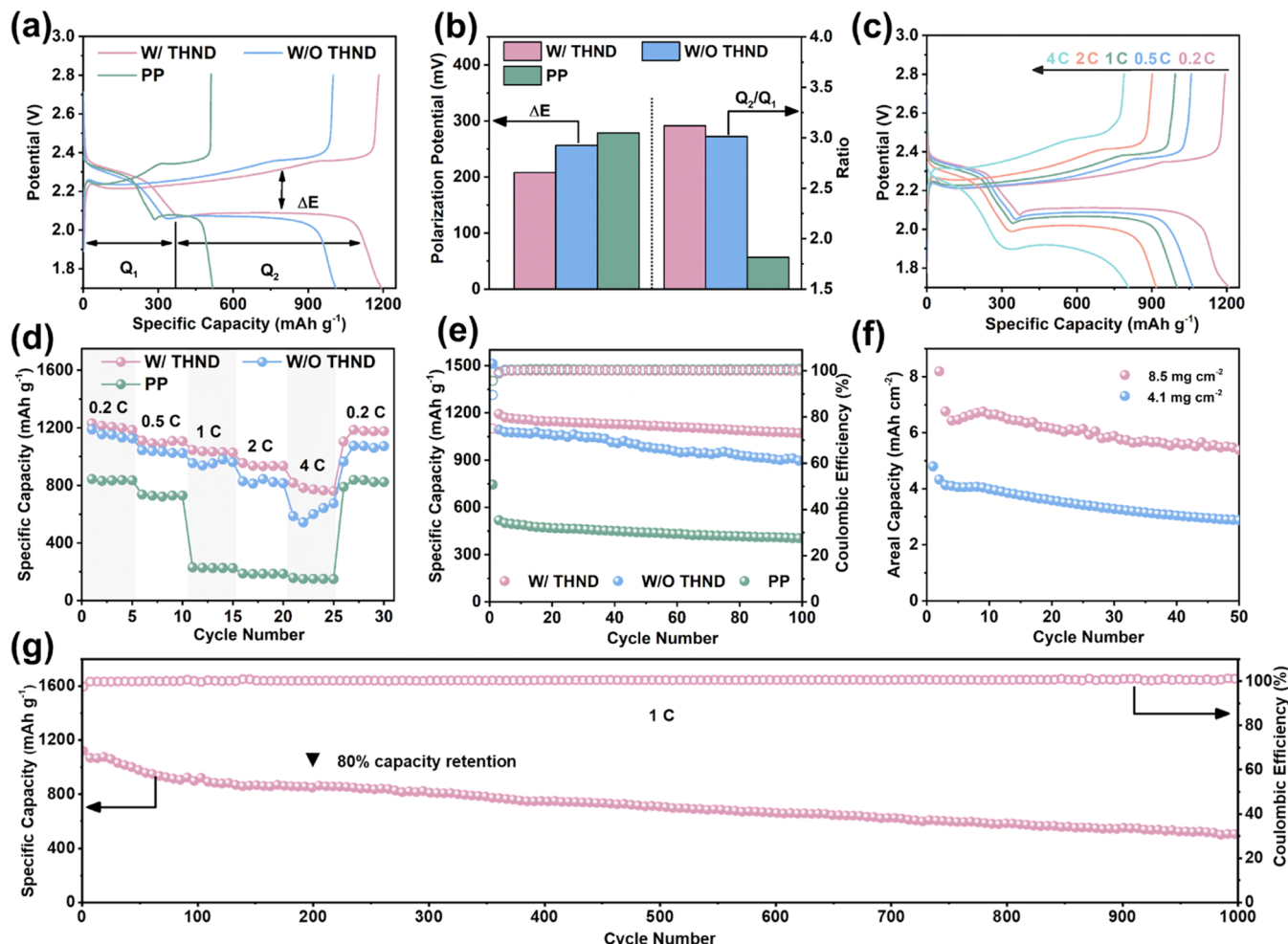


**Figure 5.** (a) Galvanostatic charge–discharge voltage profiles of Li–S batteries with different separators at a current density of 0.5C, (b)  $\Delta E$  and  $Q_2/Q_1$  calculated from the charge–discharge voltage profiles, (c) charge–discharge curves of Li–S batteries with different separators at different current rates, (d) rate performance of Li–S batteries with different separators, (e) cycling performance of Li–S batteries with different separators at 0.5C, (f) cycling performance of THNDs-based Li–S batteries under high sulfur loadings of  $4.1\text{ mg cm}^{-2}$  and  $8.5\text{ mg cm}^{-2}$  at 0.1C, and (g) long-term cycling stability at 1C.

corroborated by the activation energy ( $E_a$ ) calculated from the exchange current densities from the Tafel plots. As shown in Figure 4c, the  $E_{a1}$  value of the reduction from LiPSs to  $\text{Li}_2\text{S}$  is decreased by  $93.9\text{ kJ mol}^{-1}$  for THNDs as compared to the THNDs-free case. In the following oxidation step, the  $E_{a2}$  value of the oxidation of  $\text{Li}_2\text{S}$  to LiPSs is also greatly decreased by  $32.7\text{ kJ mol}^{-1}$ , as enabled by THNDs. The calculated results quantitatively confirm the ability of THNDs to bidirectionally accelerate the redox conversion between LiPSs and  $\text{Li}_2\text{S}$ .

The charge transfer kinetics at the LiPSs/electrocatalyst interface is another crucial indicator that influences the LiPSs redox conversion.<sup>45</sup> The smaller charge transfer resistance of the THNDs-based battery observed in the electrochemical impedance spectroscopy (EIS, Figure 4d) results indicates the facile charge transfer at the LiPS/THND interface, which is beneficial for the redox kinetics of LiPSs. To further quantitatively calculate the  $\text{Li}^+$  diffusion coefficient, CV measurements at different scan rates from  $0.1$  to  $0.5\text{ mV s}^{-1}$  were conducted (Figures 4e and S9). The calculated  $\text{Li}^+$  diffusion coefficient ( $D_{\text{Li}^+}$ ) values (Figure S13) based on the CV curves (Figures S10–S12) clearly demonstrate that the  $\text{Li}^+$  diffusion rate for batteries with THNDs is much faster. Overall, the promoted electron and ion transfer at the LiPS/THND

interface ensures the rapid redox conversion of sulfur species, which can facilitate the realization of high-rate and long-lifetime Li–S batteries.

In addition, the  $\text{Li}_2\text{S}$  nucleation and decomposition experiment also verified the enhanced bidirectional catalytic efficiency of THNDs. As shown in Figure 4f, the peak current of the cathode with THNDs ( $0.807\text{ mA}$ ) is obviously higher than that without THNDs ( $0.668\text{ mA}$ ). Moreover, the capacity of precipitated  $\text{Li}_2\text{S}$  on THNDs ( $480\text{ mAh g}^{-1}$ ) is enhanced compared to that without THNDs ( $275\text{ mAh g}^{-1}$ ), implying the facilitated  $\text{Li}_2\text{S}$  deposition induced by THNDs. Similarly, the  $\text{Li}_2\text{S}$  dissolution experiment (Figure S14) shows the higher oxidation capacity for THNDs, indicating the better dissolution efficiency of solid  $\text{Li}_2\text{S}$ .<sup>46</sup> The abovementioned results provide strong evidence that THNDs can simultaneously promote  $\text{Li}_2\text{S}$  nucleation and dissolution during both discharge and charge processes. To gain an in-depth understanding of the accelerated conversion of LiPSs by THNDs, the Gibbs free energies of stepwise sulfur reduction processes, including  $\text{S}_8$ ,  $\text{Li}_2\text{S}_8$ ,  $\text{Li}_2\text{S}_6$ ,  $\text{Li}_2\text{S}_4$ ,  $\text{Li}_2\text{S}_2$ , and  $\text{Li}_2\text{S}$ , on the surfaces  $\text{TiH}_2$  and graphene were calculated.<sup>47,48</sup> Figure 4g shows the optimized structures of the intermediates and the corresponding Gibbs free energy profiles. We can clearly see

that after the spontaneous exothermic transition from  $S_8$  to  $Li_2S_8$ , the subsequent reduction steps are thermodynamically unfavorable, especially for the process from  $Li_2S_2$  to  $Li_2S$ , which has also been recognized as the rate-determining step in the whole discharge process.<sup>49</sup> Notably, the Gibbs free energy barrier of this step is 0.82 eV for THNDs and 0.92 eV for graphene, illustrating that precipitation of  $Li_2S$  is much easier on the THNDs surface.

Benefiting from the efficient adsorption and bidirectional catalytic effect of THNDs, the electrochemical performance of Li–S batteries with THNDs-modified separators was also greatly improved. Figure 5a shows the initial discharge–charge voltage profiles of Li–S batteries with different separators at a current density of 0.5C (1C = 1675 mA g<sup>-1</sup>). The two reduction plateaus at 2.4 and 2.1 V correspond to the reduction of sulfur to soluble LiPSs ( $Q_1$ ) and the subsequent conversion of soluble LiPSs to insoluble  $Li_2S$  ( $Q_2$ ), respectively. It is obvious that the THNDs-based battery shows the largest  $Q_2/Q_1$  value with the smallest voltage polarization ( $\Delta E$ ) (Figure 5b), which indicates that THNDs can improve the utilization of sulfur by effectively capturing and catalyzing the transformation of LiPSs, as consistent with the results discussed above.<sup>50–52</sup>

The enhanced LiPSs entrapment and redox kinetics are also reflected in the excellent rate capability (Figure 5c,d). The THNDs-based batteries deliver specific discharge capacities of 1208.4, 1065.6, 1001.6, 918.1, and 807.2 mAh g<sup>-1</sup> at current densities of 0.2, 0.5, 1.0, 2.0, and 4C with the well-reserved two discharge plateaus, respectively, which are considerably higher than the counterparts. The specific capacity is recovered to 1186 mAh g<sup>-1</sup> as the current density is set back to 0.2C. Moreover, a high capacity of 1071.8 mAh g<sup>-1</sup> with a Coulombic efficiency close to 100% is retained after 100 cycles for THNDs-based batteries (Figure 5e), indicating that the introduction of THNDs can greatly alleviate the shuttle effect and improve the utilization of active substances. More impressively, a discharge capacity of 504.2 mAh g<sup>-1</sup> is still maintained after 1000 cycles at a high current density of 1C (Figure 5g), corresponding to a low capacity decay rate of 0.055% per cycle. The excellent rate capability and cyclability should be attributed to the high-catalytic THNDs with abundant active sites, which can strongly immobilize LiPS species and bidirectionally catalyze the precipitation and decomposition of  $Li_2S$  to refresh the active sites, leading to the mitigated shuttle effect and improved sulfur utilization.

To realize the practical application of Li–S batteries, high sulfur loading electrodes are indispensable.<sup>53</sup> Therefore, THNDs-based Li–S batteries with high sulfur loadings of 4.1 and 8.5 mg cm<sup>-2</sup> were investigated. As shown in Figure 5f, with a high sulfur loading of 4.1 mg cm<sup>-2</sup>, the battery can still deliver an areal capacity of 2.88 mAh cm<sup>-2</sup> after 50 cycles at a current density of 0.1C. With further increasing the sulfur loading to 8.5 mg cm<sup>-2</sup>, the battery shows an improved areal capacity of 5.38 mAh cm<sup>-2</sup> after 50 cycles, which is very competitive compared with the reported high-loading sulfur electrodes (Table S2). These results reveal the high promise of THNDs for the practical application of Li–S batteries.

## CONCLUSIONS

In summary, we demonstrated that the THNDs fabricated via facile liquid-phase exfoliation can be utilized as novel multifunctional electrocatalysts for LiPSs immobilization and conversion in Li–S batteries. The THNDs not only bring

abundant catalytically active sites but also enhance the charge transfer kinetics at the LiPS/THND interface. Moreover, the THNDs can greatly reduce the activation energy to facilitate both the precipitation and decomposition of  $Li_2S$ , which enables the suppressed shuttle effect and improved sulfur utilization. Benefiting from these advantages, the Li–S batteries assembled with THNDs exhibit outstanding electrochemical performances with a high specific capacity of 818.2 mAh g<sup>-1</sup> at 4C, a low decay rate of 0.055% per cycle after 1000 cycles, and a high areal capacity of 5.38 mAh cm<sup>-2</sup> at a high sulfur loading of 8.5 mg cm<sup>-2</sup>. Our results provide a reliable and valuable reference for the application of transition metal hydrides in the further development of practical Li–S batteries with high energy density and a long lifetime.

## ASSOCIATED CONTENT

### Supporting Information

The Supporting Information is available free of charge at <https://pubs.acs.org/doi/10.1021/acsami.1c23815>.

SEM, digital pictures of different samples, optimized adsorption configurations, Tafel plots, CV plots, and dissolution profiles of  $Li_2S$  (PDF)

## AUTHOR INFORMATION

### Corresponding Authors

Liang Cheng – Institute of Functional Nano & Soft Materials (FUNSOM), Jiangsu Key Laboratory for Carbon-Based Functional Materials & Devices, Soochow University, Suzhou 215123 Jiangsu, China;  [orcid.org/0000-0001-5324-9094](https://orcid.org/0000-0001-5324-9094); Email: [lcheng2@suda.edu.cn](mailto:lcheng2@suda.edu.cn)

Tao Cheng – Institute of Functional Nano & Soft Materials (FUNSOM), Jiangsu Key Laboratory for Carbon-Based Functional Materials & Devices, Soochow University, Suzhou 215123 Jiangsu, China;  [orcid.org/0000-0003-4830-177X](https://orcid.org/0000-0003-4830-177X); Email: [tcheng@suda.edu.cn](mailto:tcheng@suda.edu.cn)

Liang Zhang – Institute of Functional Nano & Soft Materials (FUNSOM), Jiangsu Key Laboratory for Carbon-Based Functional Materials & Devices, Soochow University, Suzhou 215123 Jiangsu, China;  [orcid.org/0000-0002-3446-3172](https://orcid.org/0000-0002-3446-3172); Email: [liangzhang2019@suda.edu.cn](mailto:liangzhang2019@suda.edu.cn)

### Authors

Tianran Yan – Institute of Functional Nano & Soft Materials (FUNSOM), Jiangsu Key Laboratory for Carbon-Based Functional Materials & Devices, Soochow University, Suzhou 215123 Jiangsu, China

Yu Wu – Institute of Functional Nano & Soft Materials (FUNSOM), Jiangsu Key Laboratory for Carbon-Based Functional Materials & Devices, Soochow University, Suzhou 215123 Jiangsu, China

Fei Gong – Institute of Functional Nano & Soft Materials (FUNSOM), Jiangsu Key Laboratory for Carbon-Based Functional Materials & Devices, Soochow University, Suzhou 215123 Jiangsu, China

Chen Cheng – Institute of Functional Nano & Soft Materials (FUNSOM), Jiangsu Key Laboratory for Carbon-Based Functional Materials & Devices, Soochow University, Suzhou 215123 Jiangsu, China

Hao Yang – Institute of Functional Nano & Soft Materials (FUNSOM), Jiangsu Key Laboratory for Carbon-Based Functional Materials & Devices, Soochow University, Suzhou

215123 Jiangsu, China; [orcid.org/0000-0002-8241-6231](https://orcid.org/0000-0002-8241-6231)

Jing Mao — School of Materials Science and Engineering,  
Zhengzhou University, Zhengzhou 450001, China

Kehua Dai — College of Chemistry, Tianjin Normal University,  
Tianjin 300387, China; [orcid.org/0000-0002-2292-7523](https://orcid.org/0000-0002-2292-7523)

Complete contact information is available at:

<https://pubs.acs.org/10.1021/acsami.1c23815>

## Notes

The authors declare no competing financial interest.

## ACKNOWLEDGMENTS

This work was supported by the Natural Science Foundation of Jiangsu Province (BK20190814), the National Natural Science Foundation of China (11905154), the Natural Science Foundation of the Jiangsu Higher Education Institutions of China (19KJAS50004), the Collaborative Innovation Center of Suzhou Nano Science and Technology, the Suzhou Key Laboratory of Functional Nano & Soft Materials, and the 111 Project. The authors thank SSRF (beamline 02B02 and 11B), NSRL (beamline 11U), and BSRF (beamline 1W1B) for the allocation of synchrotron beamtime.

## REFERENCES

- (1) Li, Z.; Wu, H. B.; Lou, X. W. Rational Designs and Engineering of Hollow Micro-/Nanostructures as Sulfur Hosts for Advanced Lithium-Sulfur Batteries. *Energy Environ. Sci.* **2016**, *9*, 3061–3070.
- (2) Bruce, P. G.; Freunberger, S. A.; Hardwick, L. J.; Tarascon, J. M. Li-O<sub>2</sub> and Li-S Batteries with High Energy Storage. *Nat. Mater.* **2012**, *11*, 19–29.
- (3) Zhou, G. M.; Yang, A. K.; Wang, Y. F.; Gao, G. P.; Pei, A.; Yu, X. Y.; Zhu, Y. Y.; Zong, L. Q.; Liu, B. F.; Xu, J. W.; Liu, N. A.; Zhang, J. S.; Li, Y. X.; Wang, L. W.; Hwang, H. Y.; Brongersma, M. L.; Chu, S.; Cui, Y. Electrotunable Liquid Sulfur Microdroplets. *Nat. Commun.* **2020**, *11*, No. 606.
- (4) Wang, J.; Li, G.; Luo, D.; Zhang, Y.; Zhao, Y.; Zhou, G.; Shui, L.; Wang, X.; Chen, Z. Engineering the Conductive Network of Metal Oxide-Based Sulfur Cathode toward Efficient and Longevous Lithium-Sulfur Batteries. *Adv. Energy Mater.* **2020**, *10*, No. 2002076.
- (5) Li, G.; Lu, F.; Dou, X.; Wang, X.; Luo, D.; Sun, H.; Yu, A.; Chen, Z. Polysulfide Regulation by the Zwitterionic Barrier toward Durable Lithium-Sulfur Batteries. *J. Am. Chem. Soc.* **2020**, *142*, 3583–3592.
- (6) Peng, H. J.; Huang, J. Q.; Liu, X. Y.; Cheng, X. B.; Xu, W. T.; Zhao, C. Z.; Wei, F.; Zhang, Q. Healing High-Loading Sulfur Electrodes with Unprecedented Long Cycling Life: Spatial Heterogeneity Control. *J. Am. Chem. Soc.* **2017**, *139*, 8458–8466.
- (7) Liang, X.; Garsuch, A.; Nazar, L. F. Sulfur Cathodes Based on Conductive Mxene Nanosheets for High-Performance Lithium-Sulfur Batteries. *Angew. Chem., Int. Ed.* **2015**, *54*, 3907–3911.
- (8) Yuan, Z.; Peng, H. J.; Hou, T. Z.; Huang, J. Q.; Chen, C. M.; Wang, D. W.; Cheng, X. B.; Wei, F.; Zhang, Q. Powering Lithium-Sulfur Battery Performance by Propelling Polysulfide Redox at Sulfophilic Hosts. *Nano Lett.* **2016**, *16*, 519–527.
- (9) Tao, X. Y.; Wang, J. G.; Liu, C.; Wang, H. T.; Yao, H. B.; Zheng, G. Y.; Seh, Z. W.; Cai, Q. X.; Li, W. Y.; Zhou, G. M.; Zu, C. X.; Cui, Y. Balancing Surface Adsorption and Diffusion of Lithium-Polysulfides on Nonconductive Oxides for Lithium-Sulfur Battery Design. *Nat. Commun.* **2016**, *7*, No. 11203.
- (10) Yao, H. B.; Zheng, G. Y.; Hsu, P. C.; Kong, D. S.; Cha, J. J.; Li, W. Y.; Seh, Z. W.; McDowell, M. T.; Yan, K.; Liang, Z.; Narasimhan, V. K.; Cui, Y. Improving Lithium-Sulphur Batteries through Spatial Control of Sulphur Species Deposition on a Hybrid Electrode Surface. *Nat. Commun.* **2014**, *5*, No. 3943.
- (11) Huang, J. Q.; Zhuang, T. Z.; Zhang, Q.; Peng, H. J.; Chen, C. M.; Wei, F. Permselective Graphene Oxide Membrane for Highly Stable and Anti-Self-Discharge Lithium-Sulfur Batteries. *ACS Nano* **2015**, *9*, 3002–3011.
- (12) Ghazi, Z. A.; He, X.; Khattak, A. M.; Khan, N. A.; Liang, B.; Iqbal, A.; Wang, J.; Sin, H.; Li, L.; Tang, Z. MoS<sub>2</sub>/Celgard Separator as Efficient Polysulfide Barrier for Long-Life Lithium-Sulfur Batteries. *Adv. Mater.* **2017**, *29*, No. 1606817.
- (13) Zeng, P.; Liu, C.; Zhao, X. F.; Yuan, C.; Chen, Y. G.; Lin, H. P.; Zhang, L. Enhanced Catalytic Conversion of Polysulfides Using Bimetallic Co<sub>2</sub>Fe<sub>3</sub> for High-Performance Lithium-Sulfur Batteries. *ACS Nano* **2020**, *14*, 11558–11569.
- (14) Tan, L.; Li, X. H.; Wang, Z. X.; Guo, H. J.; Wang, J. X. Lightweight Reduced Graphene Oxide@MoS<sub>2</sub> Interlayer as Polysulfide Barrier for High-Performance Lithium-Sulfur Batteries. *ACS Appl. Mater. Interfaces* **2018**, *10*, 3707–3713.
- (15) Yuan, C.; Yang, X. F.; Zeng, P.; Mao, J.; Dai, K. H.; Zhang, L.; Sun, X. L. Recent Progress of Functional Separators with Catalytic Effects for High-Performance Lithium-Sulfur Batteries. *Nano Energy* **2021**, *84*, No. 105928.
- (16) Feng, Y.; Wang, G.; Ju, J.; Zhao, Y.; Kang, W.; Deng, N.; Cheng, B. Towards High Energy Density Li-S Batteries with High Sulfur Loading: From Key Issues to Advanced Strategies. *Energy Storage Mater.* **2020**, *32*, 320–355.
- (17) Gu, Z. H.; Cheng, C.; Yan, T. R.; Liu, G. L.; Jiang, J. S.; Mao, J.; Dai, K. H.; Li, J.; Wu, J. P.; Zhang, L. Synergistic Effect of Co<sub>3</sub>Fe<sub>7</sub> Alloy and N-Doped Hollow Carbon Spheres with High Activity and Stability for High-Performance Lithium-Sulfur Batteries. *Nano Energy* **2021**, *86*, No. 106111.
- (18) Liu, G.; Yuan, C.; Zeng, P.; Cheng, C.; Yan, T.; Dai, K.; Mao, J.; Zhang, L. Bidirectionally Catalytic Polysulfide Conversion by High-Conductive Metal Carbides for Lithium-Sulfur Batteries. *J. Energy Chem.* **2022**, *67*, 73–81.
- (19) Lim, W. G.; Jo, C.; Cho, A.; Hwang, J.; Kim, S.; Han, J. W.; Lee, J. Approaching Ultrastable High-Rate Li-S Batteries through Hierarchically Porous Titanium Nitride Synthesized by Multiscale Phase Separation. *Adv. Mater.* **2019**, *31*, No. 1806547.
- (20) Tao, Y. Q.; Wei, Y. J.; Liu, Y.; Wang, J. T.; Qiao, W. M.; Ling, L. C.; Long, D. H. Kinetically-Enhanced Polysulfide Redox Reactions by Nb<sub>2</sub>O<sub>5</sub> Nanocrystals for High-Rate Lithium-Sulfur Battery. *Energy Environ. Sci.* **2016**, *9*, 3230–3239.
- (21) Liu, X.; Huang, J. Q.; Zhang, Q.; Mai, L. Q. Nanostructured Metal Oxides and Sulfides for Lithium-Sulfur Batteries. *Adv. Mater.* **2017**, *29*, No. 1601759.
- (22) Han, Z. Y.; Zhao, S. Y.; Xiao, J. W.; Zhong, X. W.; Sheng, J. Z.; Lv, W.; Zhang, Q. F.; Zhou, G. M.; Cheng, H. M. Engineering D-P Orbital Hybridization in Single-Atom Metal-Embedded Three-Dimensional Electrodes for Li-S Batteries. *Adv. Mater.* **2021**, *33*, No. 2105947.
- (23) Fan, L. L.; Li, M.; Li, X. F.; Xiao, W.; Chen, Z. W.; Lu, J. Interlayer Material Selection for Lithium-Sulfur Batteries. *Joule* **2019**, *3*, 361–386.
- (24) Bai, S. Y.; Liu, X. Z.; Zhu, K.; Wu, S. C.; Zhou, H. S. Metal-Organic Framework-Based Separator for Lithium-Sulfur Batteries. *Nat. Energy* **2016**, *1*, No. 16094.
- (25) Chen, B.; Wang, T. S.; Zhao, S. Y.; Tan, J. Y.; Zhao, N. Q.; Jiang, S. P.; Zhang, Q. F.; Zhou, G. M.; Cheng, H. M. Efficient Reversible Conversion between MoS<sub>2</sub> and Mo/Na<sub>2</sub>S Enabled by Graphene-Supported Single Atom Catalysts. *Adv. Mater.* **2021**, *33*, No. 2007090.
- (26) Lu, J.; Choi, Y. J.; Fang, Z. Z.; Sohn, H. Y.; Rönnebro, E. Hydrogen Storage Properties of Nanosized MgH<sub>2</sub>-0.1TiH<sub>2</sub> Prepared by Ultrahigh-Energy-High-Pressure Milling. *J. Am. Chem. Soc.* **2009**, *131*, 15843–15852.
- (27) Choi, Y. J.; Xu, Y.; Shaw, W. J.; Rönnebro, E. C. E. Hydrogen Storage Properties of New Hydrogen-Rich BH<sub>3</sub>NH<sub>3</sub>-Metal Hydride (TiH<sub>2</sub>, ZrH<sub>2</sub>, MgH<sub>2</sub>, and/or CaH<sub>2</sub>) Composite Systems. *J. Phys. Chem. C* **2012**, *116*, 8349–8358.

- (28) Ikariya, T.; Blacker, A. J. Asymmetric Transfer Hydrogenation of Ketones with Bifunctional Transition Metal-Based Molecular Catalysts. *Acc. Chem. Res.* **2007**, *40*, 1300–1308.
- (29) Oumellal, Y.; Rougier, A.; Nazri, G. A.; Tarascon, J. M.; Aymard, L. Metal Hydrides for Lithium-Ion Batteries. *Nat. Mater.* **2008**, *7*, 916–921.
- (30) Gong, F.; Cheng, L.; Yang, N. L.; Gong, Y. H.; Ni, Y. W.; Bai, S.; Wang, X. W.; Chen, M. C.; Chen, Q.; Liu, Z. Preparation of  $\text{TiH}_{1.924}$  Nanodots by Liquid-Phase Exfoliation for Enhanced Sonodynamic Cancer Therapy. *Nat. Commun.* **2020**, *11*, No. 3712.
- (31) Zhu, B.; Guan, W.; Yan, L. K.; Su, Z. M. Two-State Reactivity Mechanism of Benzene C-C Activation by Trinuclear Titanium Hydride. *J. Am. Chem. Soc.* **2016**, *138*, 11069–11072.
- (32) Luo, Y.; Wang, Q.; Li, J.; Xu, F.; Sun, L.; Zou, Y.; Chu, H.; Li, B.; Zhang, K. Enhanced Hydrogen Storage/Sensing of Metal Hydrides by Nanomodification. *Mater. Today Nano* **2020**, *9*, No. 100071.
- (33) Zhao, Z. Y.; Duan, X. B.; Zhang, L.; Che, Z. W.; Wang, K.; Zheng, B.; Wang, X. G. Elevated Electrochemical Performances Enabled by a Core-Shell Titanium Hydride Coated Separator in Lithium-Sulphur Batteries. *RSC Adv.* **2021**, *11*, 30755–30762.
- (34) Coleman, J. N.; Lotya, M.; O'Neill, A.; Bergin, S. D.; King, P. J.; Khan, U.; Young, K.; Gaucher, A.; De, S.; Smith, R. J.; Shvets, I. V.; Arora, S. K.; Stanton, G.; Kim, H. Y.; Lee, K.; Kim, G. T.; Duesberg, G. S.; Hallam, T.; Boland, J. J.; Wang, J. J.; Donegan, J. F.; Grunlan, J. C.; Moriarty, G.; Shmeliov, A.; Nicholls, R. J.; Perkins, J. M.; Grieveson, E. M.; Theuwissen, K.; McComb, D. W.; Nellist, P. D.; Nicolosi, V. Two-Dimensional Nanosheets Produced by Liquid Exfoliation of Layered Materials. *Science* **2011**, *331*, 568–571.
- (35) Shen, J. F.; He, Y. M.; Wu, J. J.; Gao, C. T.; Keyshar, K.; Zhang, X.; Yang, Y. C.; Ye, M. X.; Vajtai, R.; Lou, J.; Ajayan, P. M. Liquid Phase Exfoliation of Two-Dimensional Materials by Directly Probing and Matching Surface Tension Components. *Nano Lett.* **2015**, *15*, 5449–5454.
- (36) Zhang, Y. G.; Wang, C. M.; Liu, Y.; Liu, S. P.; Xiao, S. F.; Chen, Y. G. Surface Characterizations of  $\text{TiH}_2$  Powders before and after Dehydrogenation. *Appl. Surf. Sci.* **2017**, *410*, 177–185.
- (37) Ma, C.; Zhang, Y.; Feng, Y.; Wang, N.; Zhou, L.; Liang, C.; Chen, L.; Lai, Y.; Ji, X.; Yan, C.; Wei, W. Engineering Fe-N Coordination Structures for Fast Redox Conversion in Lithium-Sulfur Batteries. *Adv. Mater.* **2021**, *33*, No. 2100171.
- (38) Ye, J. C.; Chen, J. J.; Yuan, R. M.; Deng, D. R.; Zheng, M. S.; Cronin, L.; Dong, Q. F. Strategies to Explore and Develop Reversible Redox Reactions of Li-S in Electrode Architectures Using Silver-Polyoxometalate Clusters. *J. Am. Chem. Soc.* **2018**, *140*, 3134–3138.
- (39) Zhou, G. M.; Tian, H. Z.; Jin, Y.; Tao, X. Y.; Liu, B. F.; Zhang, R. F.; Seh, Z. W.; Zhuo, D.; Liu, Y. Y.; Sun, J.; Zhao, J.; Zu, C. X.; Wu, D. S.; Zhang, Q. F.; Cui, Y. Catalytic Oxidation of  $\text{Li}_2\text{S}$  on the Surface of Metal Sulfides for Li-S Batteries. *Proc. Natl. Acad. Sci. U.S.A.* **2017**, *114*, 840–845.
- (40) Kamphaus, E. P.; Balbuena, P. B. First-Principles Investigation of Lithium Polysulfide Structure and Behavior in Solution. *J. Phys. Chem. C* **2017**, *121*, 21105–21117.
- (41) Sun, W. W.; Li, Y. J.; Liu, S. K.; Liu, C.; Tan, X. J.; Xie, K. Mechanism Investigation of Iron Selenide as Polysulfide Mediator for Long-Life Lithium-Sulfur Batteries. *Chem. Eng. J.* **2021**, *416*, No. 129166.
- (42) Zhou, G. M.; Yang, A. K.; Gao, G. P.; Yu, X. Y.; Xu, J. W.; Liu, C. W.; Ye, Y. S.; Pei, A. E.; Wu, Y. C.; Peng, Y. C.; Li, Y. X.; Liang, Z.; Liu, K.; Wang, L. W.; Cui, Y. Supercooled Liquid Sulfur Maintained in Three-Dimensional Current Collector for High-Performance Li-S Batteries. *Sci. Adv.* **2020**, *6*, No. eaay5098.
- (43) He, J. R.; Chen, Y. F.; Manthiram, A. Vertical  $\text{Co}_9\text{S}_8$  Hollow Nanowall Arrays Grown on a Celgard Separator as a Multifunctional Polysulfide Barrier for High-Performance Li-S Batteries. *Energy Environ. Sci.* **2018**, *11*, 2560–2568.
- (44) Hua, W.; Li, H.; Pei, C.; Xia, J.; Sun, Y.; Zhang, C.; Lv, W.; Tao, Y.; Jiao, Y.; Zhang, B.; Qiao, S. Z.; Wan, Y.; Yang, Q. H. Selective Catalysis Remedies Polysulfide Shutting in Lithium-Sulfur Batteries. *Adv. Mater.* **2021**, *33*, No. 2101006.
- (45) Zhou, J. B.; Liu, X. J.; Zhu, L. Q.; Zhou, J.; Guan, Y.; Chen, L.; Niu, S. W.; Cai, J. Y.; Sun, D.; Zhu, Y. C.; Du, J.; Wang, G. M.; Qian, Y. T. Deciphering the Modulation Essence of P Bands in Co-Based Compounds on Li-S Chemistry. *Joule* **2018**, *2*, 2681–2693.
- (46) Fan, F. Y.; Carter, W. C.; Chiang, Y. M. Mechanism and Kinetics of  $\text{Li}_2\text{S}$  Precipitation in Lithium-Sulfur Batteries. *Adv. Mater.* **2015**, *27*, 5203–5209.
- (47) Chen, B.; Chao, D. L.; Liu, E. Z.; Jaroniec, M.; Zhao, N. Q.; Qiao, S. Z. Transition Metal Dichalcogenides for Alkali Metal Ion Batteries: Engineering Strategies at the Atomic Level. *Energy Environ. Sci.* **2020**, *13*, 1096–1131.
- (48) Suh, J.; Tan, T. L.; Zhao, W. J.; Park, J.; Lin, D. Y.; Park, T. E.; Kim, J.; Jin, C. H.; Saigal, N.; Ghosh, S.; Wong, Z. M.; Chen, Y. B.; Wang, F.; Walukiewicz, W.; Eda, G.; Wu, J. Q. Reconfiguring Crystal and Electronic Structures of  $\text{MoS}_2$  by Substitutional Doping. *Nat. Commun.* **2018**, *9*, No. 199.
- (49) Peng, L. L.; Wei, Z. Y.; Wan, C. Z.; Li, J.; Chen, Z.; Zhu, D.; Baumann, D.; Liu, H. T.; Allen, C. S.; Xu, X.; Kirkland, A. I.; Shakir, I.; Almutairi, Z.; Tolbert, S.; Dunn, B.; Huang, Y.; Sautet, P.; Duan, X. F. A Fundamental Look at Electrocatalytic Sulfur Reduction Reaction. *Nat. Catal.* **2020**, *3*, 762–770.
- (50) Zhang, C. Q.; Biendicho, J. J.; Zhang, T.; Du, R. F.; Li, J. S.; Yang, X. H.; Arbiol, J.; Zhou, Y. T.; Morante, J. R.; Cabot, A. Combined High Catalytic Activity and Efficient Polar Tubular Nanostructure in Urchin-Like Metallic  $\text{NiCo}_2\text{Se}_4$  for High-Performance Lithium-Sulfur Batteries. *Adv. Funct. Mater.* **2019**, *29*, No. 1903842.
- (51) Fan, C. Y.; Zheng, Y. P.; Zhang, X. H.; Shi, Y. H.; Liu, S. Y.; Wang, H. C.; Wu, X. L.; Sun, H. Z.; Zhang, J. P. High-Performance and Low-Temperature Lithium-Sulfur Batteries: Synergism of Thermodynamic and Kinetic Regulation. *Adv. Energy Mater.* **2018**, *8*, No. 1703638.
- (52) Xu, Z. L.; Lin, S.; Onofrio, N.; Zhou, L.; Shi, F.; Lu, W.; Kang, K.; Zhang, Q.; Lau, S. P. Exceptional Catalytic Effects of Black Phosphorus Quantum Dots in Shutting-Free Lithium Sulfur Batteries. *Nat. Commun.* **2018**, *9*, No. 4164.
- (53) Zeng, P.; Liu, C.; Cheng, C.; Yuan, C.; Dai, K. H.; Mao, J.; Zheng, L. R.; Zhang, J.; Chang, L. Y.; Haw, S. C.; Chan, T. S.; Lin, H. P.; Zhang, L. Propelling Polysulfide Redox Conversion by D-Band Modulation for High Sulfur Loading and Low Temperature Lithium-Sulfur Batteries. *J. Mater. Chem. A* **2021**, *9*, 18526–18536.